JOURNAL OF SOLID STATE CHEMISTRY **132,** 6–16 (1997)
ARTICLE NO. SC977383

Study of Protonic Mobility in $CaHPO_4 \cdot 2H_2O$ (Brushite) and $CaHPO_4$ (Monetite) by Infrared Spectroscopy and Neutron Scattering

L. Tortet, J. R. Gavarri,[1] and G. Nihoul

Laboratoire des Matériaux Multiphasés et Interfaces, E.A. 1357, Université de Toulon et du Var, B.P. 132, F-83 957 La Garde Cedex, France

and

A. J. Dianoux

Institute Laue Langevin, Av. des Martyrs 156 X, 38 042 Grenoble Cedex, France

Received October 1, 1996; accepted March 10, 1997

We report the first quasi-elastic neutron scattering analysis of proton mobility in the solid electrolyte $CaHPO_4 \cdot 2H_2O$ (brushite). We have studied this hydrated phosphate, in powder state, from 190 to 520 K, using an incident wavelength of 5.12 Å. The time of flight spectra are converted in $S(Q, \omega)$ structure factor and inelastic frequency distribution $P(Q, \omega)$ in the energy range 0–200 meV (0–1600 cm)$^{-1}$. A quasi-elastic contribution is clearly evidenced above room temperature; it is fitted with a jump model, involving hydrogen bonds. The quasi-elastic and inelastic scattering data are compared with FTIR results. Two kinds of motions are determined: jumps of acidic protons on hydrogen bonds and vibrations of lattice water molecules associated with the motion of their hydrogen atom on hydrogen bonds ($E_a \approx 0.145$ eV). Above 450 K the dehydration of the compound is accompanied by the appearance of a long-range diffusive motion and by the disappearance of some low-frequency inelastic bands.

I. INTRODUCTION

The presence of lattice water molecules with hydrogen bonds in brushite $CaHPO_4 \cdot 2H_2O$ and the adsorbed water molecules on its surface both condition the existence of migrating proton species involved in electrochemical devices. To study proton mobilities, complex impedance spectroscopy was carried out on composites obtained by mixing polycrystalline brushite and a powdered polymer (1). The influence of adsorbed water molecules on electrochemical activity was clearly shown. Volta experiments, using brushite as solid electrolyte, have shown that the lattice water molecules of $CaHPO_4 \cdot 2H_2O$ can also be electrolyzed as temperature increases (2). The proton motions arise from two opposite fluxes of hydrated H^+ and OH^- ions, migrating through the solid electrolyte and reacting at the electrodes.

The aim of the present study is to understand the local proton motions and, consequently, the microscopic conductivity mechanism in brushite. The vibrational spectroscopies, like infrared (IR) and inelastic neutron scattering (INS), can be used to study protonic materials, especially the hydrogen bonded solids. Quasi-elastic neutron scattering measurements (QENS) give the temporal and spatial parameters characteristic of the mobile particle dynamics. These techniques are complementary, and the information they provide can lead to a better identification of the various proton species involved in electrochemical activity.

The brushite $CaHPO_4 \cdot 2H_2O$ crystallizes at room temperature in the monoclinic space group (Cc). All the structural parameters were refined by Curry and Jones (3), using neutron diffraction: $a = 6.359$ Å, $b = 15.177$ Å, $c = 5.81$ Å, $\beta = 118.54°$, and $Z = 4$. Its crystal structure contains compact sheets, consisting of parallel chains, in which calcium ions are coordinated by six phosphate oxygens, two oxygen atoms belonging to the water molecules. Two kinds of water molecules exist in brushite: the hydrogen bonding of the two molecules differs somewhat (3–6). Figure 1 reports the structure of brushite.

II. VIBRATIONAL FTIR STUDY

The positions of the five crystallographically independent hydrogen atoms in brushite have been established by neutron diffraction (3). The acidic hydrogen is situated 1 Å from O_1, with a P–O_1 bond characterized by the longest distance value $d_{PO1} = 1.61$ Å. The two water molecules are linked somewhat differently. Several authors (3–6) have inferred

[1] To whom correspondence should be addressed.

0022-4596/97 $25.00

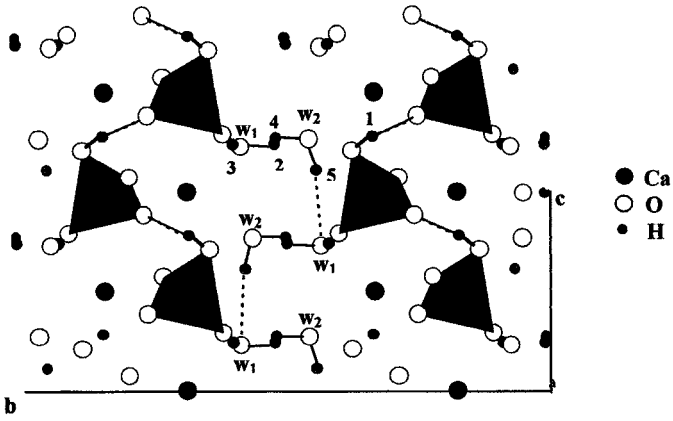

FIG. 1. Structure of brushite built from data of (3), showing PO_4 tetrahedra and H bonds.

the presence of two sorts of water molecules: one (W_1) is linked to the phosphate oxygens by strong hydrogen bonds (small O–H—O distances, 2.76 and 2.78 Å), whereas the other (W_2) presents longer and weaker hydrogen bonds (2.83 and 3.09 Å).

The comparison of the hydrogen bonds distances of 2.68, 2.76, 2.78, 2.83, and 3.09 with infrared stretching $\nu_{(OH)}$ measurement in the regions 2930, 3166, 3282, 3480, and 3541 cm^{-1} shows a fairly close correlation with the curve by Pimentel and McClellan (11). Infrared spectra reveal that the characteristic frequencies are fixed by the masses of the vibrating atoms, the molecular geometry, and the restraining forces holding the atoms in their equilibrium positions. The vibrational spectra are significantly disturbed by H bond formation. The most prominent effect of H bonding is the shift of the absorption of the O–H stretching mode $\nu_{(OH)}$ toward lower wavenumbers: the shift of $\nu_{(OH)}$, noted $\Delta\nu_{(OH)}$, is inversely related to the O–H—O distance, noted $D_{(OO)}$. This O–H—O distance is correlated inversely with O–H distance, noted $d_{(OH)}$. The bending mode $\delta_{(OH)}$ displays no obvious significant change: it is slightly shifted upward with H bond formation. But these upward shifts are smaller than the shifts of the stretching modes, and negligible in the case of brushite. Our results, presented in Table 1, are consistent with this observation.

The monetite, $CaHPO_4$, crystallizes in a triclinic unit cell $a = 6.910$ Å, $b = 6.627$ Å, $c = 6.998$ Å, $\alpha = 96.34°$, $\beta = 103.82°$, and $\gamma = 88.33°$ at 25°C, with $Z = 4$. Its structure consist of $CaHPO_4$ chains bonded together by Ca—O bonds and three types of hydrogen bonds. Two distinct sets of pairs of PO_4 units are found in each primitive cell (7).

By structure refinement based on X-ray and neutron diffraction (8–10), monetite is shown to undergo a reversible order/disorder phase transition involving H atoms only, in the range 270–290 K, depending on the presence of impurities. The low-temperature phase and the high-temperature phase are respectively consistent with the $P1$ space group and the $P\bar{1}$ space group. At room temperature, monetite mainly presents an average $P\bar{1}$ structure with one proton H_a centered on a symmetric hydrogen bond and another proton H_c disordered over two centrosymmetrically related positions (see Fig. 2: H_c and H_c'). The second hydrogen atom H_b of the structure is on an usual hydrogen bond.

In the present paper, a vibrational study by infrared spectroscopy is first presented to characterize the different hydrogen bonds. After a general review about neutron spectroscopy, we report quasi-elastic neutron scattering (QENS) studies of brushite heated at various temperatures. Finally, an inelastic neutron scattering (INS) study is discussed.

These spectral changes occur near 3500 cm^{-1} in the region of $\nu_{(OH)}$ (Fig. 3). They show the importance of qualitative criteria for H bond formation and of quantitative measurements of the H bond energy.

In monetite, only three kinds of hydrogen bonds exist in the structure, but the vibrational behavior is more complex than in brushite. Two types of PO_4 units exist in each primitive cell and induce a splitting. Differences in the bonding between H atoms and the phosphate PO_4^{3-} ions of the two different sets perturb the band splitting pattern of the vibrational spectra (12). Furthermore, as previously

TABLE 1
Hydrogen Bond Lengths (in Å) in Brushite

	H bond	$D_{(OO)}$ (Å)	$d_{(OH)}$ (Å)	IR ($\nu_{(OH)}$(Å) (cm^{-1})[a]	$\Delta\nu_{(OH)}$ (cm^{-1})
Acidic proton	O_1–H_1—O_4	2.68	1.00	2930	720
Water (1)	W_1–H_3—O_3	2.76	0.98	3166	484
	O_3—H_2–W_1	2.78	0.97	3282	368
Water (2)	O_1—H_4–W_2	2.83	0.93	3480	170
	W_2–H_5—W_1	3.09	0.9	3541	109

Note. Water oxygens are referred to as W_1 and W_2. $D_{(OO)}$ = O–H—O length, and $d_{(OH)}$ = O–H length. $\Delta\nu_{(OH)}$ is calculated according to the OH stretching mode of free water at 3650 cm^{-1}.

[a] Our work.

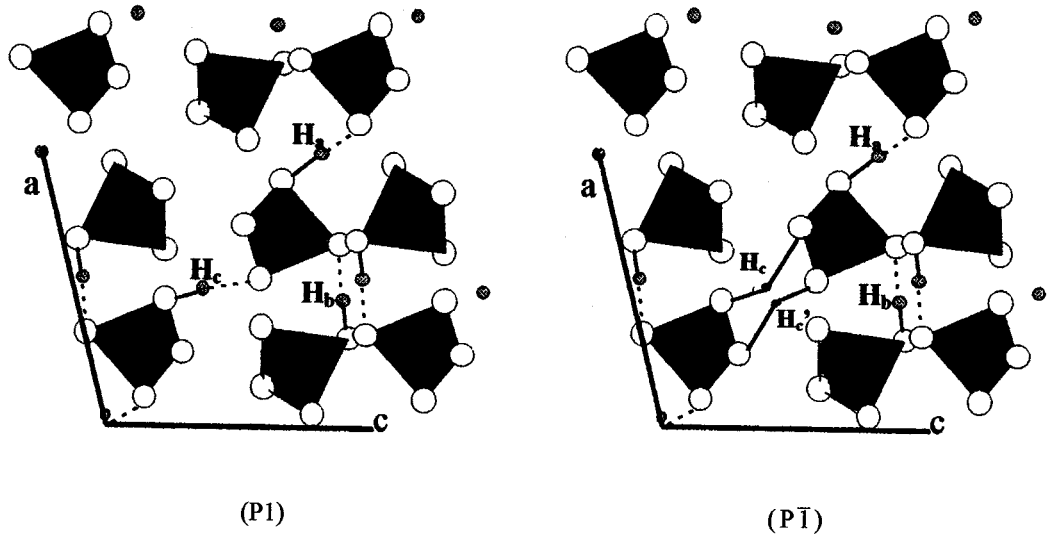

FIG. 2. Projection of the structure of the low ($P1$) and high ($P\bar{1}$) temperature phases of monetite, onto the plane normal to b built from data of (9, 10), showing PO_4 tetrahedra and H bonds.

mentioned, monetite crystallizes in a $P\bar{1}$ structure at room temperature, but the $P1$ phase should still be observed in small proportions. Catti and Ferraris (10) calculated the interatomic distances in the hydrogen bonds. Table 2 shows that these distances are different in the case of the $P\bar{1}$ model (first line), the $P\bar{1}$ model (second line), and at room temperature (third line).

The infrared stretching $\nu_{(OH)}$ observed at 3190, 2849, and 2360 cm^{-1} on the IR spectrum of monetite seems to be strongly dependent on the three types of hydrogen bonds (Fig. 4). These bands are broad, due to the disorder introduced by the different splittings and bond lengths. The H bonds are stronger in monetite than in brushite. The monetite $D_{(OO)}$ values are smaller and the shift of $\nu_{(OH)}$ consequently more important. But, because of the great number of parameters, a normal coordinate analysis with isotopic substitution will be necessary to find which H bond generates each band. It is interesting to note that $\delta_{(OH)}$ occurs as a group of bands between 1170 and 1450 cm^{-1}. Again, hydrogen bonding apparently generates the range of vibrational bands for $\delta_{(OH)}$ as for $\nu_{(OH)}$, in agreement with Pimentel and McClellan (11).

The infrared spectra of brushite and monetite at 25°C are reported in Figs. 3 and 4. The bands corresponding to the different O–H stretching modes are indicated by the name of the proton involved in the hydrogen bond: H_1, H_2, H_3, H_4, and H_5 for brushite, and H_a, H_b, and H_c for monetite.

The attributions of the main vibrational modes of brushite and monetite are reported in Table 3.

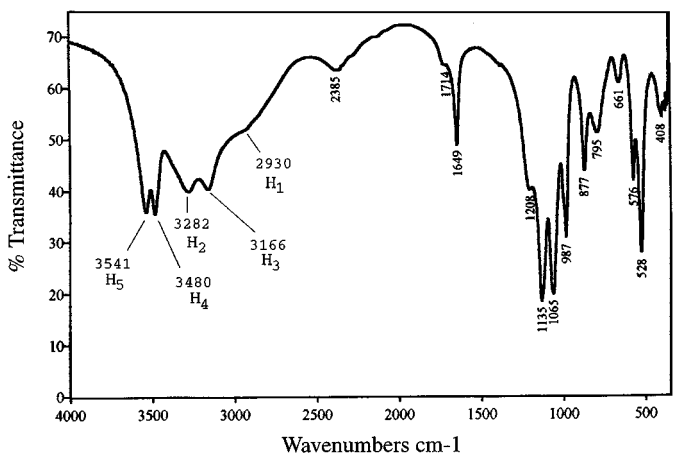

FIG. 3. Infrared spectrum of brushite.

TABLE 2
Hydrogen Bond Lengths (in Å) in Monetite ($D_{(OO)}$=O–H —O Length and $d_{(OH)}$=O–H Length), in $P1$ Model, $P\bar{1}$ Model, and at Room Temperature

H bond	$D_{(OO)}$ (Å)	$d_{(OH)}$ (Å)	IR ($\nu_{(OH)}$)(cm^{-1})
O_1–H_b—O_5	($P1$) 2.556	1.04	
	($P\bar{1}$) 2.555	0.81	3190
	(r.t.) 2.56	1.04	(broad)
O_6–H_c—O_6	($P1$) 2.724	1.05	
	($P\bar{1}$) 2.815	1.1	2849
	(r.t.) 2.658	1.15	(broad)
O_7–H_a—O_7	($P1$) 2.476	1.22	
	($P\bar{1}$) 2.474	1.24	2360
	(r.t.) 2.459	1.23	(broad)

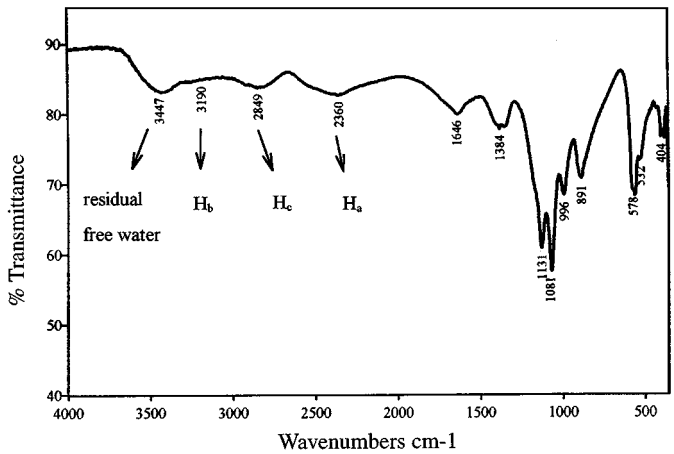

FIG. 4. Infrared spectrum of monetite.

Conclusion. In brushite, five different hydrogen bonds exist in the structure. The possible hydrogen jumps can be sorted into two families:

— jumps between two sites O—O of acidic protons (2930 cm^{-1}),

— jumps between water molecules are phosphate oxygens (long distances) (3166–3282 and 3480–3541 cm^{-1}).

Two types of water–phosphate links can then be distinguished.

In monetite, only three very short hydrogen bonds are observed: the hydrogen jumps could be assimilated to oscillations.

III. NEUTRON SCATTERING SPECTROSCOPY

The experiments have been carried out on the high flux IN6 time of flight spectrometer, at the Institute Laue Langevin (Grenoble), using an incident wavelength of 5.12 Å.

A polycrystalline sample of brushite was investigated in the 190–520 K temperature range, under vacuum. This sample was previously kept under wet atmosphere to retain adsorbed water molecules on its surface. The two types of water molecules (adsorbed and lattice water) are present in the sample at the beginning of the experiments.

In the neutron scattering technique, the scattered intensities have several origins:

— The main part comes from the proton H: the incoherent scattering cross section of hydrogen is greater than that of any other atom: $\sigma_{inc}(H) = 80.3$ barns, $\sigma_{inc}(Ca) = 0.05$ barns, $\sigma_{inc}(O) = 0.00$ barns, and $\sigma_{inc}(P) = 0.005$ barns.

— Another part comes from the other atoms with low coherent and incoherent cross sections.

— In the case of large disorder (vacancies, substitutions, distortions) an added incoherent contribution can appear which is characteristic of the disordered state of the material.

TABLE 3
Main Vibration Modes of Brushite and Monetite (FTIR Spectroscopy)

IR brushite wavenumbers (cm^{-1})	IR brushite vibration modes	IR monetite wavenumbers cm^{-1}	IR monetite vibration modes
3541–3480	O–H stretching	3447	O–H stretching
3282–3166	of lattice water molecules		of residual free water
2930	(P)O–H stretching	3190	(P)O–H stretching
		2849	
		2360	
2385	Combination		
1600–1720 (broad)	H–O–H bending and rotation of residual free water	1600–1700 (broad)	H–O–H bending and rotation of residual free water
1649 (thin)	H–O–H bending of lattice water molecules		
1208	P–O–H in-plane bending	1450–1300 (broad)	P–O–H in-plane bending
1135	P–O stretching	1170 (sh)	P–O stretching
1065		1131	
		1081	
987	P–O stretching	996	P–O stretching
877	P–O(H) stretching	891	P–O(H) stretching
795	P–O–H out-of-plane bending		
661	Water librations		
576	O–P–O(H)	578	O–P–O(H)
528	bending mode	532	bending mode
408	O–P–O(H) bending mode	420	O–P–O
		404	bending mode
370[a]	Water translation		
363[a]	Lattice modes		
337[a]			
		285[a]	Lattice mode

[a] From literature.

III.1. Thermal Evolution of Neutron Scattering Intensities

In our case, the brushite initial crystals are assumed to be ordered except for protons which can vibrate, jump, or migrate at long distances. To estimate the signals due to the proton presence and mobility, the analysis of the total scattered intensity has been carried out. In Fig. 5, the evolution during heating of the total scattered intensity (TSI), quasi-elastic scattering intensity (QESI) due to proton mobility at large distances, and inelastic scattering intensity (InSI) due to collective and local vibrations are reported.

(i) The TSI curve exhibits a strong decrease above 400 K: this indicates a significant departure of protons due to the dehydration process.

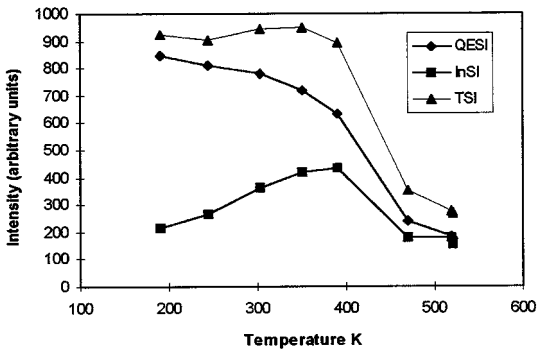

FIG. 5. Quasi-elastic scattering intensity (QESI), inelastic scattering intensity (InSI), and total scattered intensity (TSI) as a function of temperature.

(ii) The QESI curve slowly decreases up to 400 K and then exhibits a significant decrease above 400 K: this latter evolution is obviously correlated with the lattice water proton departure.

(iii) The InSI curve first increases then exhibits a strong decrease due to the elimination of protons; the first increase could be due to the thermal activation of phonons and vibrations (brushite lattice) and proton contributions in the brushite crystals.

The different steps occurring during heating are the following:

— Between 245 and 350 K, the sample is constituted of brushite and adsorbed water.

— Between 350 and 390 K, adsorbed water is eliminated.

— Above 420 K, the brushite is decomposed into monetite: the lattice water molecules are eliminated. To ensure that a complete dehydration was achieved we have realized three experiments at 520 K. A measurement was also carried out on the obtained monetite at 303 K.

III.2. Quasi-elastic Neutron Scattering (QENS) Spectroscopy

After reviewing the classical models available in the literature, we use a fitting procedure to determine the effective QENS signals. Then, the modeling of the experimental QE signals is presented and discussed.

III.2.1. Definitions and Review of Elemental Models

Definitions. The intermediate scattering law is given by

$$I_{\text{inc}}(Q,t) = \frac{1}{N}\sum_{i=1}^{N} \langle \exp\{iQ\cdot R_i(t)\}\exp\{-iQ\cdot R_i(0)\}\rangle, \qquad [1]$$

where N is the number of particles in the unit cell and R the position of the atom i at time t.

The scattering function $S_{\text{inc}}(Q,\omega)$ is the time-Fourier transform of $I_{\text{inc}}(Q,t)$:

$$S_{\text{inc}}(Q,\omega) = \frac{1}{2\pi}\int_{-\infty}^{\infty} I_{\text{inc}}(Q,t)\exp(-i\omega t)\,\mathrm{d}t. \qquad [2]$$

In the time of flight spectra, the separation of the elastic contribution has been obtained by a fitting procedure involving one Lorentzian function folded with experimental resolution,

$$S_{\text{fit}} = A\delta(\omega) + B\mathscr{L}(\omega)$$

where $\delta(\omega)$ is a Dirac function and $\mathscr{L}(\omega)$ the Lorentzian function.

$$S_{\text{fit}} = A\delta(\omega) + B\frac{1}{\pi}\frac{h}{h^2+\omega^2}$$

$$\int S_{\text{fit}}\mathrm{d}\omega = A + B \qquad [3]$$

The half-width at half-maximum (HWHM) of the Lorentzian (h in Eq. [3]), and the elastic incoherent structure factor (EISF), corresponding to the fraction of the elastic intensity, i.e., the ratio of the elastic scattering to the total scattering I (quasi-elastic I_{QE} plus elastic I_{E}) are the leading parameters. The QES signals are deduced from the total intensity using a vanadium standard, which has no coherent contribution.

$$\text{EISF} = \frac{A}{A+B} = A_0(Q) \qquad [4]$$

The EISF gives the geometry of the motion of the mobile particles.

$$I = \int S_{\text{fit}}\,d\omega = A + B = Fe^{-Q^2\langle u^2\rangle}$$

$$\log I = \log F - Q^2\langle u^2\rangle \qquad [5]$$

The slope of the line $\log I = f(Q^2)$ gives the $\langle u^2\rangle$ values, the mean square amplitudes of vibration.

Review of simple models. In our compounds, different types of motions can occur:

— continuous jump diffusion among sites (i.e., H migrations or H_2O free migrations),

— jumps among two sites (i.e., jumps along a O–H—O bond),

— rotations (i.e., OH rotations in free water molecules),

— complex surface motions of adsorbed molecules (i.e., H_2O surface motions including diffusion and rotation).

The *translational continuous self-diffusion* is described by

$$S_{\text{inc}}(Q\omega) = \frac{1}{\pi}\frac{DQ^2}{(DQ^2)^2 + \omega^2}, \qquad [6]$$

where the HWHM IS DQ^2.

The *long-range jump diffusion model* was developed by Chudley and Elliot (13). It was extended to hydrogen diffusion in metals. It deals with an atom diffusing by jumps to nearest neighbor sites on a Bravais lattice and corresponds to the case in which the jump time is negligible compared to the residence time τ_0. The jump model leads to scattering laws in which the quasi-elastic broadening at a large Q value (HWHM) deviates from the DQ^2 law:

$$\Delta\omega(Q) = \frac{1}{\tau_0}\left[1 - \frac{\sin\ Qd}{Qd}\right]. \qquad [7]$$

In the case of Brownian motion, the jump length d of the diffusing particle is assumed to be small compared to the distance r of this particle from the origin. It results in

$$\Delta\omega(Q) = DQ^2, \quad \text{with} \quad D = \frac{1}{6}\frac{d^2}{\tau_0}.$$

This model is based on the following hypotheses. For a time interval τ_0, an atom remains on a given site, vibrating about a center of equilibrium, building up a thermal cloud. After this time, the atom moves rapidly to another site, in a negligible jump-time. The length of the jump vector between these two sites, d, is assumed to be much larger than the dimension of the thermal cloud.

In the *jump model among two equivalent sites* (*short-range motions*), the scattering law is

$$S(Q,\omega) = A_0(Q)\delta(\omega) + A_1(Q)\frac{1}{\pi}\frac{2\tau}{4 + \omega^2\tau^2}$$

$$A_0(Q) = \frac{1}{2}\left(1 + \frac{\sin Qd}{Qd}\right) \qquad (8)$$

$$A_1(Q) = \frac{1}{2}\left(1 - \frac{\sin Qd}{Qd}\right),$$

where d is the jump distance between the two sites, τ^{-1} is the jump rate probability (independent of Q), and $A_0(Q)$ is the EISF.

In the *rotational diffusion* on the surface of a sphere S of radius R, the effective mean HWHM varies with Q, and the EISF is given by (14)

$$A_0(Q) = \left(\frac{\sin QR}{QR}\right)^2. \qquad [9]$$

Water has been the subject of numerous studies for a long time. However many problems are not yet completely resolved. In the water model, a molecule executes an oscillatory motion for a mean time τ_0. Then it diffuses by continuous motion for a mean time τ_1. In the limit of small momentum transfers or small τ_0 values, $Q^2D\tau_0 \ll 1$, the expression of HWHM of the quasielastic peak reduces to $\Delta\omega = DQ^2$, which is the expression of the broadening predicted by the simple diffusion theory. In contrast, if $Q^2D\tau_0 \gg 1$, the broadening tends to the asymptotic value $\Delta\omega = 1/\tau_0$, independent of the momentum transfer. This model can be compared to the diffusive jump model: τ_0 is the lifetime of the oscillatory motion which can be identified with the residence time of the Chudley–Elliot model. The time τ_0 is much greater than the period of the oscillatory motion and, during this time, the motion of the molecules is very similar to that observed in the solid state. The study of water in its supercooled state is reported by Teixeira *et al.* (15).

III.2.2. Experimental Determination of the QENS Signals

Probable jump lengths. Proton motions have already been the subject of many studies (16–18) and, more precisely, in the case of the potassium phosphate KH_2PO_4 was interpreted in terms of thermally activated hopping motion of a classical particle, by a model assuming that the protons are randomly distributed on the two sites separated by 0.32 Å along the hydrogen bonds.

In the case of the brushite and of the monetite all the hydrogen atoms are localized on hydrogen bonds. The hydrogen bond distances and the lengths of the jumps susceptible to occur are reported in Table 4, according to

TABLE 4
Hydrogen Bond Distances and Lengths of the Jumps Expected to Occur in Brushite and Monetite

Lengths (Å)	O–H—O	O–H	H—O	Jump
Adsorbed water	2.7	1	1.7	0.7
Brushite				
Acid proton	2.68	1	1.68	0.68
Lattice water	3.09	0.9	2.16	1.26
	2.83	0.93	1.9	0.97
	2.78	0.97	1.81	0.84
	2.76	0.98	1.78	0.8
Monetite	2.66[a]	1.15	1.51	0.47
	2.56	1.04	1.52	0.48
	2.46	1.23	1.23	0[b]

[a] The hydrogen H_c is delocalized on two sites, on two possible hydrogen bonds (10) and can give rise to a disorder.

[b] The hydrogen is observed by Catti *et al.* (9, 10) to be localized at the centre of the O–O distance.

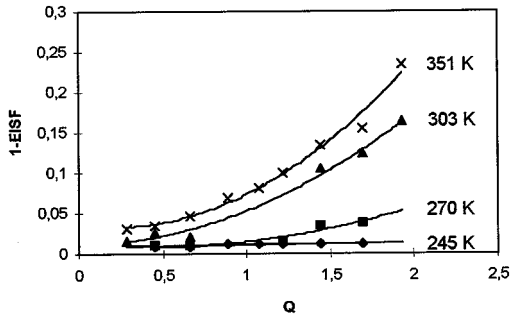

FIG. 6. Elastic to total intensity ratio (1-EISF) for different temperatures before the departure of the adsorbed water, as a function of the momentum transfer Q (Å^{-1}).

(3) and (10). The jump values are approximate because the bond angles are not taken into account.

We can note that the lengths of the probable jump calculated in the case of brushite are longer than that in the case of monetite: thus, they are expected to be less probable.

Experimental QE signals. The normalized quasi-elastic intensity (1-EISF) is plotted as a function of the momentum transfer, Q, at various temperatures in Fig. 6. The HWHM of the Lorentzian is plotted as a function of Q at various temperatures in Fig. 7.

The quasi-elastic intensity at $Q = 2$ Å^{-1} increases continuously from 0.01 at 245 K to 0.24 at 351 K.

Above 360 K, the (1-EISF) curves decrease: the fraction of mobile species decreases with the elimination of the two types of water molecules. The thermal evolution of the EISF curves is an indication that the number of particles able to undergo jumps is temperature dependent.

The HWHM is quasi-constant in the full Q range below 390 K. This means that the quasi-elastic scattering is mainly associated with localized motions and that long-range translational motions are not clearly evidenced. Moreover, it is observed that the HWHM increases with temperature; this means that the corresponding process is thermally activated.

Finally, the large values found for the EISF seem to indicate that only a small fraction of hydrogen is mobile on the time scale set by the resolution of the instrument (10 μeV or $\sim 10^{-10}$ s).

One could think that all hydrogen atoms might be involved in a small amplitude rattling about their site and this could explain the weakness of the QE intensity. Such a motion is thermally activated and the associated HWHM increases with temperature.

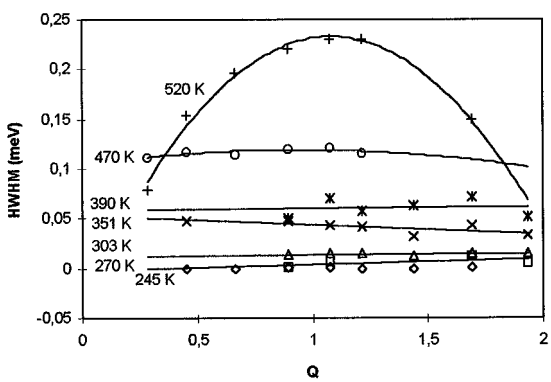

FIG. 7. HWHM of the Lorentzian as a function of the momentum transfer Q (Å^{-1}). Up to 470 K, the HWHM is constant. At 520 K (decomposition temperature) the HWHM first increases (like in a DQ^2 behavior) and then decreases.

III.2.3. Modeling of the QE Signals

A better fit of the experimental data is given by the following model: the protons are assumed to oscillate between the two minima of the hydrogen bridge double-well potential. Taking into account the vibrational component of the proton motion in the usual way (i.e., by extracting a Debye–Waller factor), the EISF, $A_0(Q)$, for a powder sample is

$$A_0(Q) = \frac{1}{2}\left[1 + \frac{\sin(Qd)}{Qd}\right], \qquad [10]$$

where d is the distance between the two proton sites.

According to these hypotheses, we have calculated different parameters, characteristic of the motions:

— The slopes of the curves of the logarithm of the total intensity as function of Q^2 give the mean square amplitudes of vibration $\langle u^2 \rangle$ (Eq. [5]).

— The HWHM values are quasi-constant: the broadening tends to the asymptotic value $\Delta\omega = 1/\tau$, independent of the momentum transfer. The corresponding residence times have been calculated.

— The values of the jump distances have been obtained by fitting the EISF curves with Eq. [10].

All results are presented in Table 5.

Between 390 and 523 K, the sample is a mixture of brushite and monetite. No intermediate compound has been observed (2). The two kinds of water molecules are simultaneously eliminated. During the decomposition, the QENS results cannot be considered as representative of a stable phase.

The vibration amplitudes increase with temperature, and the residence times decrease. The $\langle u^2 \rangle$ values are between 0.023 and 0.04 Å^2 as T increases, corresponding to the mean square amplitude of the proton vibration on an hydrogen bond, calculated approximately to be 0.038 Å^2 by Tomkinson (19), at room temperature. Curry and Jones (3) and Catti *et al.* (9) determined the Debye–Waller factors of the atoms

TABLE 5
Mean Parameters of the Proton Motions in Brushite and Monetite

Samples	$\langle u^2 \rangle$ (Å^2)	$\langle u \rangle$ (Å)	HWHM (meV)	τ(s)	d (Å)
Bru 245 K	0.024	0.154			
Bru 270 K	0.024	0.154	0.01	$4.1\ 10^{-10}$	0.36
Bru 303 K	0.030	0.172	0.015	$2.8\ 10^{-10}$	0.78
Bru 350 K	0.037	0.193	0.04	$1.0\ 10^{-10}$	0.95
Bru 390 K	0.041	0.202	0.06	$6.9\ 10^{-11}$	0.87
Mo 303 K[a]	0.031	0.175	0.05	$8.3\ 10^{-11}$	0.54

[a] Result of brushite dehydration.

in brushite and monetite, respectively. They obtained large amplitude factors for W_1, W_2, and the hydrogen atoms. The mean values of $\langle u^2 \rangle$ which can be obtained from their results are the following:

— for W_1 and W_2, $\langle u^2 \rangle_{300\,K} \approx 0.024$ Å^2,

— for the hydrogen atoms, $\langle u^2 \rangle_{300\,K} \approx 0.035$ Å^2.

These values are consistent with our results.

Below 303 K, hydrogen atoms do not jump; they can only undergo some rattling in their potential well ($d =$ 0.36 Å at 270 K), leading to a negligible QE signal.

At 303 K, hydrogen atoms can jump. The d value (0.78 Å), which corresponds to the jump length, seems to be related to the jump distances involved in the hydrogen bonds of the adsorbed water and of the acidic lattice proton. At room temperature, only the shorter jumps can be realized.

At 350 K, the obtained d value (0.95 Å) is an average of all the jump lengths expected in brushite. All hydrogen atoms are now excited by thermal energy.

At 390 K, the departure of adsorbed water begins: it is difficult to interpret the results. The mean square amplitude of vibration has increased, and consequently, the residence time τ has decreased.

Above 390 K, the shapes of the HWHM curves as function of Q (Fig. 7) can be fitted by the equation of the jump diffusion model

$$\Delta\omega(Q) = \frac{1}{\tau_0}\left[1 - \frac{\sin\ Qd}{Qd}\right].$$

The obtained value of the length jump is on the order of 4 Å, and the residence time is of 2.2×10^{-11} s, at 520 K. This jump length can correspond to the distance between the lattice water molecules, which are progressively eliminated at these temperatures. Their departure gives rise to large motions in the water molecule region (see the structure of brushite in Fig. 1). The calculated mean square amplitudes of vibration $\langle u^2 \rangle$ are 0.13 and 0.14 Å^2 at 473 and 530 K, respectively.

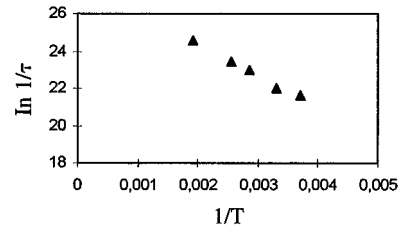

FIG. 8. Logarithm of $1/\tau$ as a function of $1/T$, for brushite between 270 and 520 K. The slope of the curve gives $E_a = 0.145$ eV.

The third experiment at 520 K shows that the signal can be attributed to the apparition of the monetite. At this temperature, the decomposition is complete.

Finally, when monetite has been cooled down to 303 K, the new EISF curve can be fitted with the proposed jump model. The obtained d value (0.54 Å) is a little larger than the calculated jump distance (0.48 Å). However, a certain disorder existing in monetite at room temperature, due to the delocalized position of the H_c hydrogen, can induce this greater value and can explain the elevated values of vibration amplitude and of the HWHM. The hydrogen atoms are more susceptible to jump in monetite than in brushite because the jump distances are smaller.

The value of the activation energy E_a is calculated with $\tau^{-1} = \tau_0^{-1} \cdot e^{-E_a/RT}$. In Fig. 8, the logarithm of $1/\tau$ is plotted as a function of $1/T$, for temperatures between 270 and 520 K. The obtained value for E_a is 0.145 eV ($\tau_0 = 1.01 \times 10^{-12}$ s).

Remarks. 1. In the temperature range 270–520 K only one activation energy is observed: this indicates that the same proton species are involved in the motions. At 245 K, this motion seems to be blocked.

2. The activation energy of monetite has been independently calculated with the data of monetite at 303 and 520 K: the obtained value is 0.043 eV ($\tau_0 = 1.59 \times 10^{-11}$ s). Thus, the activation energy of the acidic protons is small.

Conclusion. In brushite, two different types of motions could exist:

— hydrogen jumps on the hydrogen bonds, and

— vibration of hydrogen on the hydrogen bonds probably associated with the total water molecule oscillation in its well.

In monetite, only one type of motion seems to appear: the jump of the acidic protons along the hydrogen bonds.

III.3. Inelastic Neutron Scattering

In this section, we present the results obtained from inelastic neutron scattering experiments, corresponding to vibrations and phonons in brushite and monetite.

The incoherent inelastic neutron scattering (INS) data are comparable to those observed in optical vibrational infrared spectroscopy. The IN6 spectrometer allows us to work in the 0–1600 cm^{-1} spectral range, for temperatures above 300 K. The intensity of IR signals is of electronic origin, being related to the magnitude of the change in dipole moment, and so is governed by symmetry selection rules. The intensity in INS is due to nuclear interactions and no symmetry selection rules apply. An INS experiment gives the scattered intensity at different values of Q and ω.

The INS intensity of a vibrational model, $S(Q,\omega)$, is related to the mean square displacement of the scattering atom, $\langle u^2 \rangle$ by (19)

$$S(Q,\omega) \propto Q^2 \langle u^2(\omega) \rangle e^{-2Q^2\langle u^2 \rangle}.$$

The study of the vibrations of hydrogen bonds using INS has been the subject of recent reviews (19–25). Usually, the existence of H_3O^+ and $H_5O_2^+$ ions is assumed for hydrated compounds. Tomkinson (19) has presented a recent inelastic incoherent neutron scattering work involving the study of the H bond vibrations. He mentioned the case of strong hydrogen bonds ($2.44 < D_{(OO)} < 2.8$ Å) and of lattice water molecules.

In the general case of a polyatomic unit, with n atoms of species i, concentration c_i, and scattering cross section $\sigma_i^{inc} = 4\pi b_{i,inc}^2$, the neutron-weighed density of state can be defined (26) as

$$p_N(\omega) = \frac{\bar{M}}{\bar{\sigma}} \sum_{i=1}^{n} c_i \frac{\sigma_i}{m_i} p_i(\omega),$$

where $\bar{M}$ is the average atomic mass and $\bar{\sigma}$ the average atomic cross section. The density of states $p_N(\omega)$ is obtained using an iterative procedure (27), which works with a user-defined number of vibrational modes, characterized by five parameters (the scattered mass, the frequency, the intensity, the cut-off frequency, and the shape of the peak). The Debye–Waller factor and the multiphonon contribution are estimated and used to give a model which is fitted to the experimental one. When the fit is satisfactory, $p(\omega)$ is obtained after subtraction of the multiphonon contribution. In our modeling, we have used four vibrational modes corresponding to the vibrational modes of the entities PO_4, Ca, O, and H. The spectra are normalized to 1, in the energy range from 0 to 220 meV.

The inelastic frequency distributions $P(\bar{Q},\omega)$ in the energy range 0–200 meV (0–1600 cm^{-1}) of brushite and monetite, recorded at 303 K, are shown in Figs. 9 and 10. The spectral attributions of the observed bands are reported in Table 6. The other spectra, obtained at the other temperatures, present no intermediate compound and no new band revealing different proton motions. We have interpreted the spectra in terms of the presence of hydrogen phosphate groups, of water molecule in the case of brushite, and of two strong hydrogen bonds ($D_{(OO)}$ distance short) in the case of monetite. The INS spectra of the two compounds are dominated by intense bands above 800 cm^{-1}, which may be assigned to the in-plane deformation vibration and to the stretching mode of the P–O–H group.

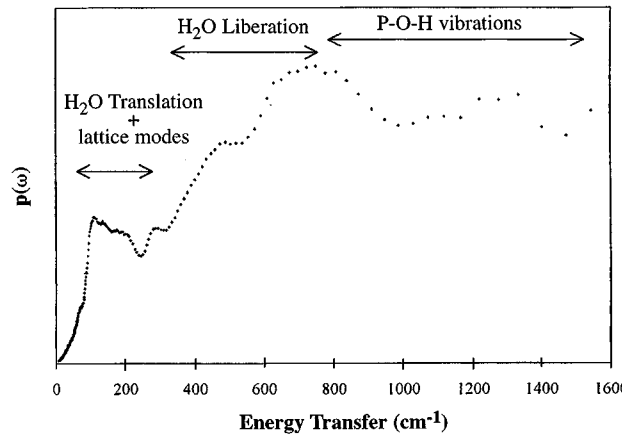

FIG. 9. INS spectrum of $CaHPO_4 \cdot 2H_2O$ in the range 0–200 meV (0–1600 cm^{-1}), recorded at 303 K. Lattice H_2O molecules translational motions are observed in the range 50 to 350 cm^{-1}.

III.3.1. Water Motions (Brushite)

We can observe a strong decrease in the intensity in the 400 to 770 cm^{-1} spectral range after dehydration of brushite into monetite (see Fig. 11, where the two spectra of brushite and monetite are superposed).

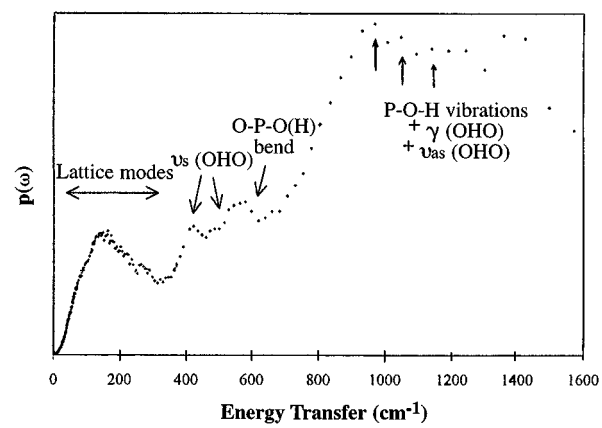

FIG. 10. INS spectrum of $CaHPO_4$ in the range 0–200 meV (0–1600 cm^{-1}), recorded at 303 K. No lattice water motion, only lattice modes in the 50–350 cm^{-1} range. (O–H–O) vibration modes of short hydrogen bonds.

TABLE 6
Main Vibrational Modes of Brushite and Monetite Observed in the INS Spectra, with the IN6 Spectrometer

INS brushite wavenumbers (cm^{-1})	INS brushite vibration modes	INS monetite wavenumbers (cm^{-1})	INS monetite vibration modes
1230	P–O–H in-plane bending	1400 (s)	P–O–H in-plane bending
		1250 (s)	γ (OHO)
1130	P–O stretching	1170 (s)	P–O stretching
		1022 (s)	γ (OHO)
860	P–O(H) stretching	930 (s)	P–O(H) stretching
770 (s, br)	H_2O librations		
		575	O–P–O(H) bending
500 (br)	H_2O librations	480	ν_s (OHO)
		420	ν_s (OHO)
306 (m)	H_2O translation (local)		
		268 (w)	Lattice mode
225	H_2O translation		
210	(local)		
195	+ lattice modes		
155 (lattice)			
130		146	Lattice mode
75 (lattice)			

Note. w, weak; m, medium; s, strong; br, broad; OHO, hydrogen bond.

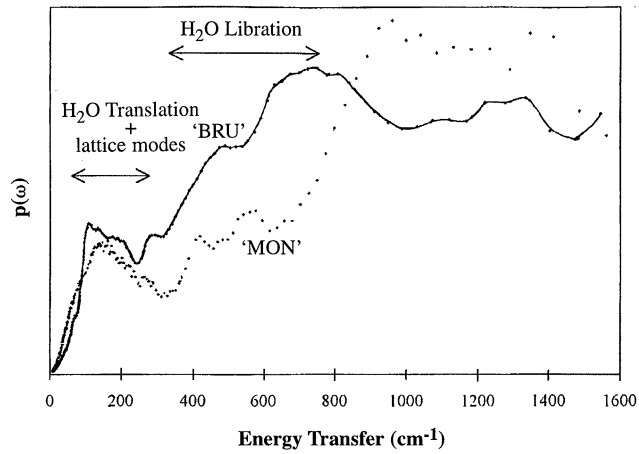

FIG. 11. Superposition of the INS spectra of brushite and monetite.

Librational and translational modes, for frequencies characteristic of water, exist in brushite. In the low-frequency range, several maxima of the density of states are observed at 130, 210, and 306 cm^{-1}, which can correspond to the translational motion of water.

Above 400 cm^{-1}, individual librational motions of H_2O (19) are expected, as torsional (τ), rocking (ρ), and wagging (ω) modes. However, the resolution decreases significantly with increasing energy transfer, when using a cold neutron TOF instrument like IN6. The bands become broad. Nevertheless, two broad bands may be distinguished with maxima at 500 and 770 cm^{-1}.

III.3.2. Short Hydrogen Bonds (Monetite)

Two very strong hydrogen bonds exist in monetite (as a result of brushite dehydration), with short distances $D_{(OO)}$ (2.46 and 2.56 Å). In this kind of compound, where $D_{(OO)}$ distances are short, OHO modes of vibration appear. Jones and Roziere (21) studied a hydrogen bond with an oxygen–oxygen distance of 2.44 Å. They expected four internal vibrations of this hydrogen bond: the symmetric and antisymmetric stretching modes (ν_s, ν_{as}), and the in- and out-of-plane deformation vibrations [δ (OHO) and γ (OHO)].

On our monetite INS spectra, the symmetric stretching modes ν_s, absent in infrared spectroscopy, appear as sharp and medium intensity maxima at 420 and 480 cm^{-1}, while the deformation vibrations are barely discernible in the region 1200–1400 cm^{-1}.

Another INS study of intramolecular H bonds has located the γ (OHO) bands (28). These bands are never mixed with other molecular modes, and their position can be correlated with $D_{(OO)}$ (Å) distances. Detailed IR work (29) provided a correlation: $D_{(OO)}$ (Å) $= 3.01\text{–}4.4 \times 10^{-4}\,\gamma$(OHO) cm^{-1}, for $D_{(OO)}$ distances greater than 2.44 Å. We have calculated these positions in the case of the two short hydrogen bonds of monetite: for the H bonds 2.46 and 2.56 Å long, the γ (OHO) bands should be localized at 1250 and 1022 cm^{-1}, respectively, as can be observed on our INS spectra (Fig. 10).

The bands of monetite are more intense than the brushite bands above 900 cm^{-1}: thus, their amplitude of vibration is greater. This fact tends to confirm that the monetite hydrogen atoms are more mobile. Another feature can increase the intensity in this region: the strongly hydrogen-bonded systems usually produce very strong absorption in the mid-frequency range.

Finally, we cannot observe any intense signal that could be assigned to H_3O^+.

III.3.3. Conclusion

The oscillations of the lattice water molecules in their oxygen well should be associated with two features:

— the local proton jumps observed from QES analyses, which are thermally activated, ($E_a = 0.145$ eV) could be the result of translational motions of W_1 and W_2 molecules, and

— the inelastic signals observed in the phonon distribution are directly linked with the existence of the lattice water molecules, observed between 130 and 800 cm^{-1}.

If one assumes that the force constant of a H bond is around 10 $N\,m^{-1}$, the associated oscillation should be characterized by

$$\tilde{\nu} = \frac{1}{2\pi c}\sqrt{\frac{K}{\mu}} = 106\ \mathrm{cm}^{-1},$$

with $\mu = 18\ \mathrm{g\,mol}^{-1}$. This value only gives a rough indication of the frequency range of such water vibrations in the structural well.

IV. CONCLUSION

We have attempted to compare the types of information obtained from infrared spectroscopy and incoherent quasi-elastic and inelastic neutron scattering applied to hydrogen bonded brushite and monetite. These spectroscopic methods can be used in a combined and complementary approach for the identification of the local proton motions. However, they have provided no evidence for proton transfer on long distance and for the concomitant formation of oxomium ions, H_3O^+.

At intermediate temperature, localized motions are responsible for quasi-elastic signals in brushite:

— jumps on hydrogen bonds of the "acidic protons";

— vibrations of lattice water molecules, associated with the motion of their hydrogen atom on the hydrogen bonds.

At higher temperatures, these localized motions temporarily transform into long-range diffusion, with the departure of lattice water molecules.

The activation energy ($E_a = 0.145$ eV) is the same on the whole temperature range.

After heating, fast jumps of the proton, on the short hydrogen bonds, exist in monetite (with $E_a = 0.043$ eV).

The inelastic analysis has permitted some attribution of low-frequency water vibration modes in brushite.

REFERENCES

1. L. Tortet, J. R. Gavarri, and G. Nihoul, *J. Solid State Ionics* **89,** 99 (1996).
2. L. Tortet, J. R. Gavarri, G. Nihoul, J. M. Fulconis, and F. Rouquerol, *Eur. J. Solid State Inorg. Chem.* **33,** 1199 (1996).
3. N. A. Curry and D. W. Jones, *J. Chem. Soc., A* 3725 (1971).
4. E. E. Berry and C. B. Baddiel, *Spectrochim. Acta A* **23,** 2089 (1967).
5. I. Petrov, B. Soptrajanov, N. Fuson, and J. R. Lawson, *Spectrochim. Acta A* **23,** 2637 (1967).
6. F. Casciani and R. A. Condrate, *Spectroscopy Lett.* **12** (10), 699 (1979).
7. B. Dickens, J. S. Bowen, and W. E. Brown, *Acta. Crystallography. B* **28,** 797 (1971).
8. W. A. Denne and D. W. Jones, *J. Cryst. Mol. Struct.* **1,** 347 (1971).
9. M. Catti, G. Ferraris, and A. Filhol, *Acta Crystallography B* **33,** 1223 (1977).
10. M. Catti, G. Ferraris, and S. A. Mason, *Acta Crystallogr. B* **36,** 254 (1980).
11. G. C. Pimentel and A. L. McClellan, "The Hydrogen Bond", p. 2390. Freeman, San Francisco, 1960.
12. F. Casciani and R. A. Condrate, *J. Solid State Chem.* **34,** 385 (1980).
13. C. T. Chudley and R. J. Elliot, *Proc. Phys. Soc.* (*London*) **77,** 353 (1961).
14. V. F. Sears, *Can. J. Phys.* **45,** 237 (1967).
15. J. Teixeira, M. Bellisent-Funel, S. H. Chen, and A. J. Dianoux, *Phys. Rev. A.* **31,** 1913 (1985).
16. J. R. Gavarri, P. Garnier, P. Boher, A. J. Dianoux, G. Chedeville, and B. Jacq, *J. Solid State Chem.* **75,** 251 (1988).
17. S. Shibata and S. Ikeda, *J. Phys. Soc. Jpn.* **61**(2), 441 (1992).
18. S. Ikeda, Y. Noda, H. Sugimoto, and Y. Yamada, *J. Phys. Soc. Jpn.* **63**(3), 1001 (1994).
19. J. Tomkinson, *Spectrochim. Acta A* **48,** 329 (1992).
20. J. Tomkinson, *in* "Neutron Scattering at a Pulsed Source" (C. Winsley, Ed.). Hilger, Bristol, 1988.
21. D. J. Jones and J. Rozière, *Solid State Ionics* **61,** 13 (1993).
22. D. Rousselet and A. Potier, *J. Chim. Phys.* **70,** 873 (1973).
23. D. J. Jones, J. Tomkinson, J. Penfold, and J. Rozière, *J. Mol. Struct.* **197,** 113 (1989).
24. D. J. Jones and J. Rozière, *Solid State Ionics* **35,** 115 (1989).
25. R. C. T. Slade, C. Forano, H. Pressman, J. M. Nicol, A. Peraio, and G. Alberti, *J. Mater. Chem.* **2,** 583 (1992).
26. W. Marshall and S. W. Lovesey, "Theory of Thermal Neutron Scattering." Oxford Univ. Press, London, 1971.
27. A. Fontana, F. Rocca, M. P. Fontana, B. Rosi, and A. J. Dianoux, *Phys. Rev. B* **41**(6), 3778 (1990).
28. T. Brun, J. Howard, and J. Tomkinson, *Spectrochim. Acta A* **42,** 1209 (1986).
29. A. Novak, *Struct. Bonding* (*Berlin*) **18,** 177 (1974).